Journal of Photochemistry and Photobiology A: Chemistry 234 (2012) 83–90

Contents lists available at SciVerse ScienceDirect

Journal of Photochemistry and Photobiology A: Chemistry

journal homepage: www.elsevier.com/locate/jphotochem

Optical trapping and polarization-controlled scattering of dielectric spherical nanoparticles by femtosecond laser pulses

Anwar Usman*, Wei-Yi Chiang, Hiroshi Masuhara*

Department of Applied Chemistry and Institute of Molecular Science, National Chiao Tung University, Hsinchu 30010, Taiwan

ARTICLE INFO

Article history:
Received 23 October 2011
Received in revised form
19 November 2011
Accepted 21 November 2011
Available online 12 January 2012

Keywords:
Optical trapping
Dielectric nanoparticles
Lorentz force

ABSTRACT

We present optical trapping behavior of 50-nm-sized polystyrene beads, suspended in water medium, by femtosecond pulsed laser beam. In addition to a higher number of nanoparticles trapped at the focal spot by the ultrashort laser pulses compared with that by continuous-wave laser, the nanoparticles are scattered out of the focal spot by the laser pulses to the surrounding area. The scattered particles form a partially opened folding fan-shaped bright locus in two opposite directions, in an alternating manner, perpendicular to the laser polarization. To understand those phenomena, we analyzed radiation (gradient and scattering) force of femtosecond laser pulses and their temporal force exerted on the dielectric spherical nanoparticles by taking into account the impulsive peak power and the axial component of electric light field produced by high numerical aperture of objective lens. We show that the axial electric field is responsible for lateral components of the scattering and temporal forces, and hence, controls the scattering directions of the Rayleigh particles. These findings provide important information about the dynamic optical trapping of the Rayleigh particles by highly focused ultrashort laser pulses.

1. Introduction

One of the successful applications of mode-locked lasers is the ultrafast time-resolved spectroscopies, which provide the absorption, vibrational, or emission spectra of atoms or molecules on extremely short time scales after their excitation with ultrashort laser pulses. The research group of Prof. M. Martin is one of pioneers who have utilized transient absorption spectroscopy to decipher the dynamics and mechanisms of fundamental photo-induced processes [1]. Their reports on the insights of driving forces and primary occurring events in the photo-induced dynamics of various chromophores, photoactive proteins, or biomimetics are important advances in our understanding of the photo-processes, particularly the functionality of the biomaterials in relation with their electronic structures [2–7].

Another important laser application is optical trapping (also called optical tweezers), exploiting the optical gradient force, which can confine micrometer to submicrometer-sized objects in the focal spot [8,9]. In this phenomenon, a high numerical aperture lens is necessarily required to focus tightly the continuous-wave (cw) laser beams into a diffraction-limited spot size [10,11]. With its potential ability of non-destructive tool to immobilize, reorient, and transfer the micro-to-submicrometer sized dielectric or metallic particles, this technique has been widely applied in various fields of sciences with target materials ranging from small particles [12], polymers [13,14], clusters of amino acids [15–19], to biological substances [20], and has become indispensable in single-molecule measurements [21,22].

Recently, the optical trapping technique is further developed by utilizing ultrashort laser pulses. By the femtosecond laser pulses, optical trapping of micrometer-sized silica spheres was found to be as effective as cw optical tweezers, and trap stiffness was related to average power of the laser pulses [23]. With the ultrashort laser pulses, however, several phenomena have been revealed, including optical trapping of as small as a few nm-sized CdTe quantum dots or the depositions of CdS nanoparticles with grain size down to 25 nm [24,25]. For the trapping of gold nanoparticles by laser pulses, the trapping site splits up into two equivalent positions around the focal center, demonstrating that high nonlinear optical susceptibility of the target materials can modify the shapes of gradient force and trapping potential [26]. More recently, the femtosecond laser pulses with the power less than 200 mW has been successfully applied to confine an individual polystyrene bead with a diameter of a few tens of microns (the particle sizes within the framework of geometrical optics regime), but the microparticle was

* Corresponding authors at: Department of Applied Chemistry and Institute of Molecular Science, National Chiao Tung University, 1001 Ta Hsueh Rd., Hsinchu 30010, Taiwan. Tel.: +886 3 5712121x56595.
E-mail addresses: usman@faculty.nctu.edu.tw (A. Usman), masuhara@masuhara.jp (H. Masuhara).

1010-6030/$ – see front matter © 2012 Elsevier B.V. All rights reserved.
doi:10.1016/j.jphotochem.2011.11.015

pushed away from the trapping site when the focal position was shifted to its downstream surface due to secondary convergence of the laser pulses that reduces water breakdown threshold [27].

In this article, we report on an experimental study exploring the trapping behavior of the dielectric spherical nanoparticles (50-nm-diameter polystyrene beads), suspended in liquid water medium, by femtosecond laser pulses tightly focused by high numerical aperture lens. We show that as compared with the cw mode, the laser pulses can trap a larger number of nanoparticles. In addition, the laser pulses induce nanoparticle flows out of the focal spot in two opposite directions, in an alternating manner, controlled by the laser polarization. To understand this phenomenon, we evaluate both radiation (gradient and scattering) and temporal forces (the latter is also called pulse radiation force) by adopting Lorentz force of fundamental Gaussian beam exerted on Rayleigh particles [10,28], and by applying scattering cross section value of the nanoparticles obtained based on Mie theory [29]. We demonstrate that the axial electric field produced by the high numerical aperture objective lens is responsible for the present novel phenomenon.

2. Experimental

2.1. Optical setup

To experimentally exemplify the trapping behavior of the nanoparticles by femtosecond laser pulses, we developed an experimental setup based on an inverted microscope (Olympus IX71), as shown in Fig. 1. We used a 800-nm fundamental mode of Ti:sapphire (Tsunami; Spectra Physics) laser beam, which can be operated in cw or femtosecond-pulse mode, acting as the trapping beam. When it was operated in the pulse mode, the pulse duration was compressed by a pair of prisms to be about 90 fs, and the repetition rate was 80 MHz. The polarization direction of the laser beam was controlled by a half-wave plate before the beam was collimated and expanded to ~5 mm in diameter by a pair of positive lenses with focal length being 100 and 200 mm, respectively. The beam then was focused through an objective lens (60×, NA = 0.90) at normal incidence into a sample cell, which was placed on the sample stage of the microscope. The light power after the objective lens was controlled in the range of 0.10–0.35 W. The beam waist, ω_0, at the focal spot was calculated to be 460 nm, equivalent to the calculated radius when the beam intensity of its first Airy pattern falls to $1/e^2$ of the maximum value.

2.2. Sample cell and detection system

The sample cell consisted of a silicon chamber (1 mm thickness) sandwiched between two cover-glass plates (Matsunami). The inner well of the chamber (10 mm in diameter) was filled with colloidal solution containing spherical polystyrene beads (PolyScience; radius = 25 nm, density = 1.06 g/cm^3) suspended in distilled water (refractive index = 1.33 at room temperature). Concentration of the polystyrene beads was 3.79×10^{14} particles/mL. The refractive index of the polystyrene nanoparticles at 800 nm wavelength was calculated by Cauchy dispersion relation to be 1.59 [30].

The sample cell containing the dielectric spherical nanoparticles was illuminated by white light (λ = 400–750 nm) from a halogen lamp passing through a cardioid immersion dark field condenser lens (Olympus; U-DCW NA = 1.4–1.2). The elastic light scattering originated from the laser trapping beam was completely cut by a shortwave-pass filter with transmission at 380–720 nm (Semrock; Brightline 750/SP) in front of charge-coupled device (CCD) camera (JAI; CV-A551R E). With such a setup only the scattering light from halogen lamp by the nanoparticles was collected by the objective lens, and was detected by using the CCD camera running at 30 interlaced frames per second. Thus, the detected light intensity can be related mainly to the scattering light intensity, although there is possibly a very minor contribution of three-photon excited fluorescence of the bare polystyrene beads due to nonlinear optical effects if such the fluorescence wavelength is longer than 380 nm to pass the shortwave-pass filter. The positions of the nanoparticles were associated with the image of the scattering light detected by the CCD camera. The resolution of the image in the lateral direction was 94 nm per pixel, and our observation layer was limited within the axial resolution of the objective lens (calculated to be approximately 1.8 μm).

3. Results

With the laser trapping beam operated in the femtosecond pulse mode at the average power of 350 mW, we observed a brighter scattering light at the focal spot compared with the surrounding area. We should note that such bright scattering light was never observed in a neat solvent. In addition to scattering light at the focal spot, bright locus of scattered polymer beads, just like multiple shooting stars, from the focus spot to the surrounding area was also observed. The bright locus was shaped like a partially opened folding fan along two opposite directions, in an alternating manner, perpendicular

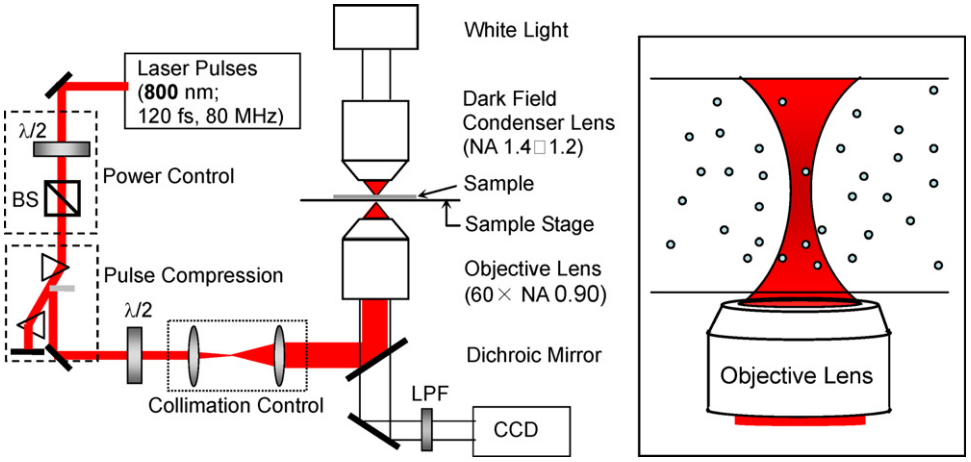

Fig. 1. Schematic diagram of the experimental set-up; λ/2 is halfwave plate, BS is beam splitter, and LPF is low pass filter. Inset is a schematic illustration of the sample cell containing the colloidal solution of nanoparticles.

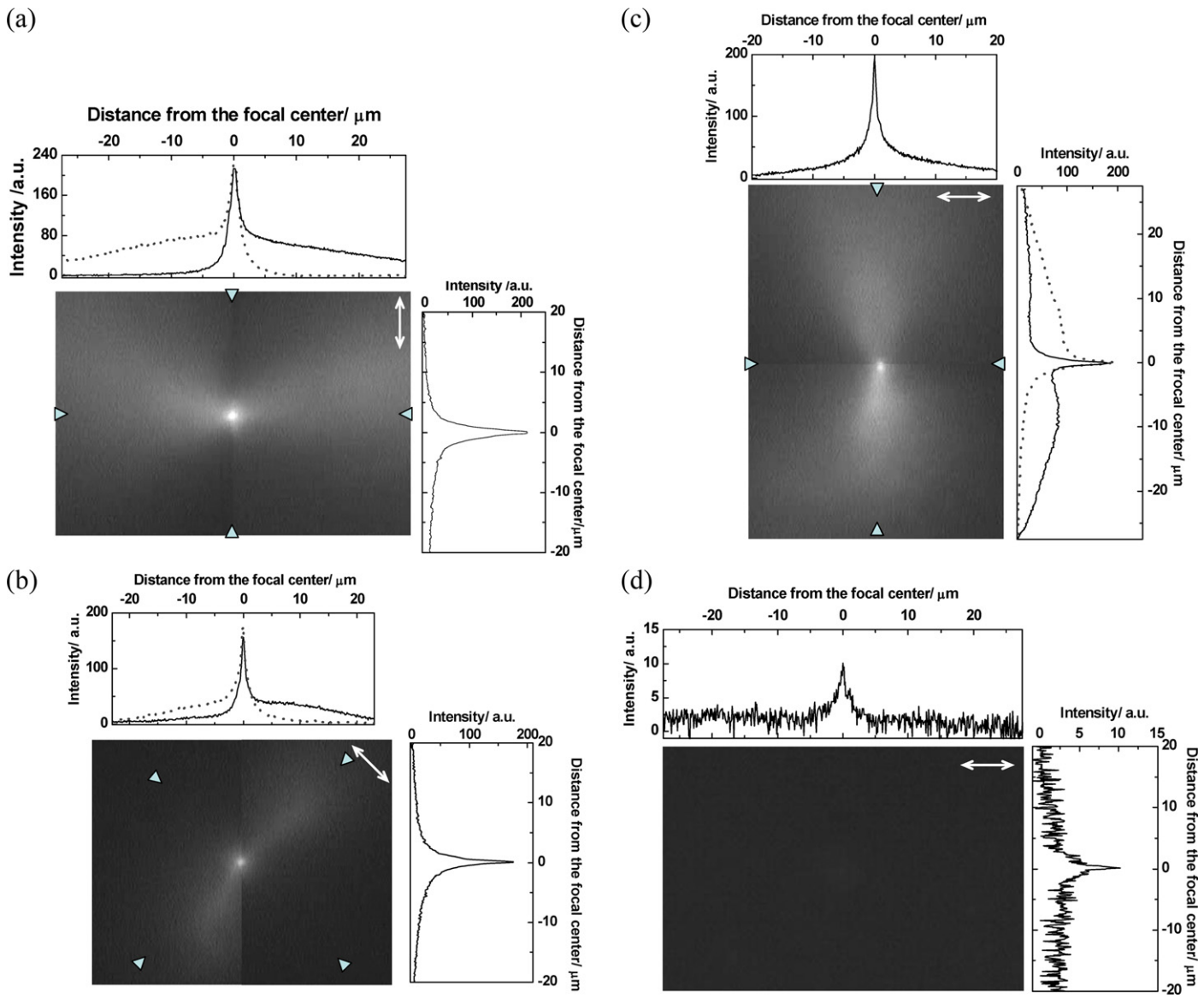

Fig. 2. A combination of two halves of two different image frames showing optical trapping and scattered polystyrene nanoparticles by femtosecond-pulse modes and showing their optical trapping by cw Ti:sapphire laser beams (λ = 800 nm). (a)–(c) A sharp scattering light at the focal spot and bright locus of scattered polymer beads from the focus spot to the surrounding area towards two opposite directions in an alternating manner perpendicular to the laser polarization direction of femtosecond laser pulses, indicating the optical trapping of polystyrene nanoparticles at the focal spot and nanoparticle flows along the two opposite directions. The laser power for each case is 350 mW after the objective lens. Arrow in each panel indicates polarization direction of the laser beam. The line profiles in each panel were taken from one cursor passing through the focal center to the opposite cursor, parallel and perpendicular to the polarization direction. The two line profiles (solid and dotted lines) perpendicular to the polarization direction are related to the two alternating directions of the scattering light. (d) An unstable and low scattering light intensity from the focal spot of cw laser beam at the same laser power. Arrow in the panel indicates polarization direction, and the line profiles were taken from parallel and perpendicular to the polarization direction.

to the polarization direction. Such the event occurred randomly, and simultaneous bright locus along the two opposite directions like a pair of two partially opened folding fans was never observed. Thus, we show the bright locus along the two opposite directions by combining two halves of different video frames in Fig. 2(a)–(c) (the original videos are given in Videos S1–S3 in Supporting information for more details). Since the scattering lights detected in the video image represent the positions of the nanoparticles, we therefore extracted the profiles of scattering light intensity passing through the focal center as shown in each panel. Such line profile parallel to the polarization direction shows clearly a single sharp peak with an approximately 1.6 μm full width at half maximum at the focal spot, whereas that perpendicular to the polarization direction indicates the additional bright locus of scattered polymer beads along the two opposite directions in an alternating manner. The intensity of the bright locus is comparable to each other. When the laser beam was operated in the cw mode at the same laser power, only a tiny scattering light at the focal spot was observed under the similar experimental conditions, but there were no any observable bright locus of scattered polymer beads from the beam center to the surrounding area. An image frame under the cw-mode laser irradiation is shown in Fig. 2(d) (the original video is given in Video S4 in Supporting information). The line profiles passing through the focal center parallel and perpendicular to the polarization direction reveal that the scattering light at the laser focal spot of the cw mode is very low.

By varying the laser power, the threshold of the femtosecond laser pulses to induce observable scattering light at the focal point and bright locus along the two opposite directions was observed at 264 mW for the highly concentrated nanoparticle solution. We also found that the concentration of the nanoparticles was a

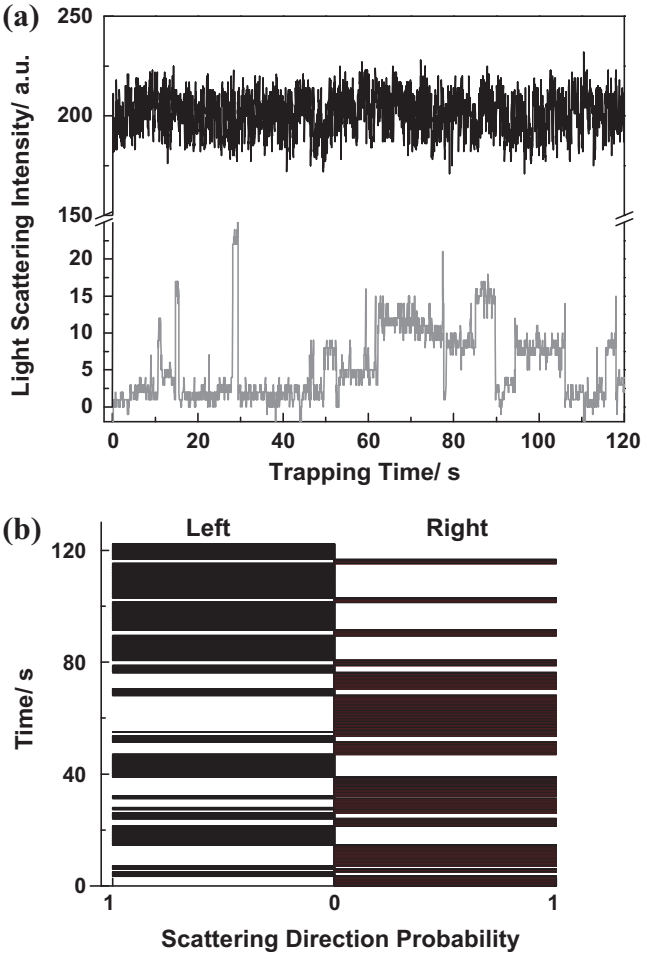

Fig. 3. (a) Time-dependent line profile intensity under femtosecond-pulse (black line) and cw mode (gray line). (b) The typical time-dependent event when bright locus of scattered polymer beads from the focus spot is along the two alternating left and right directions within the observation window of 120 s. Experimental information for data shown in the figures (a) and (b) are related to those in Fig. 2(a).

crucial parameter to observe the bright locus. Under the laser pulses at the average power of 350 mW, the bright locus was not observed when the colloidal solution was diluted by a factor of 4, equivalent to the concentration of 0.95×10^{14} particles/mL. We consider that, under the same optical conditions, the fourfold dilution led to severe reductions in the trapping rate, size of trapped assembly, and number of scattered nanoparticles, giving no images of bright locus.

The temporal evolutions of scattering light intensity at the focal spot when the laser beam was operated in femtosecond-pulse or cw mode are shown in Fig. 3(a). In contrast to high intensity of scattering light when the laser beam was operated in the pulse mode, low intensity, unstable, and fluctuated scattering light intensity was observed under the cw mode. In comparison, the scattering light intensity is about one order higher when the laser beam was operated in the pulse mode than that under cw mode.

Further, in Fig. 3(b) we show the plot of the temporal random distribution of the event, where the bright locus was observed along one of the two alternating directions perpendicular to the polarization of the femtosecond laser pulses, for the observation window about 120 s. The bright locus emerged in one direction on the timescale of seconds before they changed into the opposite direction, and they continued in the same way. The probability and total duration of the bright locus along the two alternating directions almost balanced each other.

4. Discussion

4.1. Optical trapping and nanoparticle flows

Extracting the intensity of scattering light by line profile is one of useful practical ways to identify the spatial position of nanoparticles in colloidal solution. Typically, a sharp light intensity at the focal spot in the line profiles can be attributed to nanoparticles accumulated by laser trapping, and the number of trapped nanoparticles is associated with the light intensity [31]. Similarly, the existence of such single and sharp peak intensity from the spherical polystyrene beads under the femtosecond laser pulses, as shown in Fig. 2, indicates the possible of a single trap site at the focal spot. Such a single trap site is commonly observed in conventional optical trapping experiments [8,32], but it is in contrast to the trap split of 60-nm sized gold nanoparticles by the femtosecond laser pulses on the same level of average laser power [26]. It is noteworthy that since the third-order nonlinear optical susceptibility is responsible and sensitive to split the trap site into two equivalent positions shifted from the beam axis, the lower third-order susceptibility of polystyrene nanoparticles (0.8×10^{-8} esu) [33] as compared with that of gold nanoparticles (5×10^{-8} esu) [34] is the reason for the polymer nanoparticles having no clear observable nonlinear optical effect on the trap site.

Here, we interpret our experimental results as follows. When a nanoparticle enters the effective trapping area by diffusion, gradient force due to a steep gradient of optical intensity of the highly focused ultrashort laser pulses is exerted on the nanoparticle, and the force drags the nanoparticle towards the single trap site at the focal center. A stable trapping can only be achieved when the gradient force overcomes scattering force, and the characteristic stiffness of optical trap should be proportional to the laser intensity, as it has been reported for the trapping laser in cw mode [21,35]. For the ultrashort optical pulses, in particular, in addition to the gradient and scattering forces, we also have to consider temporal force within the pulse duration, which is defined as instantaneous Lorentz force at the time over the entire duration of the pulse envelope [36–38]. In this case, the gradient force of the laser pulses should overcomes the scattering and their temporal forces to achieve a stable trapping. Considering the sizes of the nanoparticles and beam waist, multiple nanoparticles can be trapped in the single potential minimum at the focal spot, and the scattering light intensity is proportionally enhanced with the number of trapped nanoparticles at the trap site. Thus, monitoring such the scattering light intensity, similarly to monitoring a stepwise behavior of fluorescence intensity increase in optical trapping of 100- or 200-nm-sized dye-doped polystyrene nanoparticles by cw laser beam [39], would provide the information on the number of nanoparticles entering the trap site. However, the video frames in our experiment are saturated within the first integrating time, hindering a precise observation on the exact number of the optically trapped nanoparticles. Nevertheless, based on the scattering light intensity at the focal spot (Fig. 3(a)) we could roughly estimate the number of trapped nanoparticles to be at least one order higher when the laser is operated in the femtosecond pulse mode compared with that under cw mode on the same averaged laser power.

Since the optical trapping potential can only filled by a certain number of nanoparticles, additional nanoparticles entering the trapping site should push and replace the nanoparticles occupying the trapping site. The trapped nanoparticles can also escape and release themselves from the trapping site by diffusion during the interval period between two laser pulses. The nanoparticles escaped from the optical trapping site are readily pushed farther away from the focal center by scattering or temporal forces. Although one single pulse may not be able induce the migration of

nanoparticles along the way as they are observed in this present work, but since the laser pulses are repeatedly introduced at the pulse repetition rate of 80 MHz into the highly concentrated nanoparticles, we consider that multiple nanoparticles are scattered with the high frequency on the same direction. With this mechanism, the stable quantity of nanoparticles at the trapping site is maintained, resulting in the constant intensity of line profiles observed at the trapping site, while multiple nanoparticles are continuously scattered out of the focal spot making their motions as a kind of nanoparticle flow, which is observed as the multiple shooting stars from the focal spot to the surrounding area forming a partially opened folding fan-shaped bright locus. Interestingly, the nanoparticle flows are along two opposite directions, in an alternating manner, controlled by the laser polarization. In the following, we show that such the polarization-controlled nanoparticle flows can be attributed to the existence of lateral component of scattering and temporal forces.

4.2. Radiation and temporal forces acting on a dielectric spherical nanoparticle

Let us consider the fundamental mode of Gaussian beam propagating without distortion in a medium containing dielectric spheres. The beam is tightly focused by a high numerical aperture objective lens, converging to a near-diffraction-limited size with a focal waist being ω_0, and then reexpanding. Here, we consider that Lorentz force acts on a dielectric spherical nanoparticle due to interactions between light electric field and induced dipole moment of the polarizable dielectric sphere. The induced polarization can be approximately expressed as, $\mathbf{P} = \chi\mathbf{E}$, where χ is the electric susceptibility. For a uniform dielectric sphere, the susceptibility is isotropic and the polarization $\mathbf{P}$ is parallel to $\mathbf{E}$. Thus, the gradient force, related to spatial Lorentz force, exerted on the nanoparticles can be expressed as [28]

$$\mathbf{F}_{\text{grad}} = [\mathbf{P}\cdot\vec{\nabla}]\mathbf{E} = \frac{1}{2}\alpha\vec{\nabla}|E|^2 \tag{1}$$

where $\alpha = 4\pi n_m^2\varepsilon_0 a^3[(m^2-1)/(m^2+2)]$ is the polarizability of an individual nanoparticle in the Rayleigh regime, ε_0 is vacuum permittivity, a is the radius of the nanoparticle, and $m = n_p/n_m$ is the relative refractive index of the particle (n_p) to medium (n_m). Another component in the radiation force is the scattering force due to momentum transfer of light exerting on the dielectric sphere, as given by

$$\mathbf{F}_{\text{scatt}} = \left(\frac{n_m\sigma_p}{c}\right)\langle\mathbf{E}\times\mathbf{H}\rangle_t \tag{2}$$

where σ_p is the scattering cross section of a nanoparticle, c denotes the speed of light in vacuum, and $\langle\mathbf{E}\times\mathbf{H}\rangle_t$ is the time-averaged energy flux of the laser pulses. The temporal force is given by [36–38]

$$\mathbf{F}_{\text{temp}} = \mu_0\partial_t\langle\mathbf{P}\times\mathbf{H}\rangle = \alpha\mu_0\partial_t\langle\mathbf{E}\times\mathbf{H}\rangle \tag{3}$$

where μ_0 is vacuum permeability. The character and magnitude of this temporal force depend strongly on the pulse duration [40], and this force is obviously zero for the cw laser beams.

It is noteworthy that in our experimental case, for wavelength of laser beam $\lambda = 800$ nm and beam waist $\omega_0 = 460$ nm, beam divergence half-angle (defined as $\theta = \lambda/\pi n_m\omega_0$) is calculated to be $\sim 24^\circ$. Consequently, the axial vector field of the plane-polarized Gaussian beams tightly focused by such an objective lens can not be neglected [41,42]. If we assume the focal plane is located at the xy-plane ($z = 0$), and the carrier frequency and pulse duration of the laser pulses is ω and τ, respectively, the linearly polarized electric field parallel to the x-axis can be expressed as $E_{x0} = E_0\exp[i\omega t - \xi^2]\exp[-\tilde{t}^2]$ (where $\xi = x/\omega_0$ and $\tilde{t} = t/\tau$). We note that the electric field along the y-axis is zero in the lowest order approximation of the paraxial Gaussian beam [41,43], and the axial electric field along the z-axis can be derived using $E_{z0} = (-i/k)\partial_x E_{x0}$, and one obtains

$$E_{z0} = -iK\xi\,E_0\exp[i\omega t - \xi^2]\exp[-\tilde{t}^2] \tag{4}$$

where $k = 2\pi/\lambda$ and $K = 2/k\omega_0$. By considering that the axial component is a phase quadrature, the electric field on the x-axis is given by [26], $\mathbf{E} = E_0(\hat{x}\cos\omega t + \hat{z}K\xi\sin\omega t)\exp[-\xi^2]\exp[-\tilde{t}^2]$ (where $\hat{x}$ is the unit vector along the x-axis, and $\hat{z}$ is the unit vector of z-axis or along the beam propagating direction). With the corresponding magnetic field of the laser pulses, $\mathbf{H} = n_m\varepsilon_0 c(\hat{x}E_{z0} + \hat{y}E_{x0})$, the gradient, scattering, and temporal forces exerting on a nanoparticle at the focal plane, as presented in Eqs. (1)–(3), can be therefore expressed as follows:

$$\mathbf{F}_{\text{grad}} = -\hat{x}\alpha E_{x0}^2\left[\frac{\xi}{\omega_0} - \frac{1}{2}\frac{K^2\xi}{\omega_0} + \frac{K^2\xi^3}{\omega_0}\right] \tag{5}$$

$$\mathbf{F}_{\text{scatt}} = \hat{z}\left(\frac{n_m^2\sigma_p\varepsilon_0}{2}\right)E_{x0}^2 + \hat{y}\left(\frac{K^2\xi^2 n_m^2\sigma_p\varepsilon_0}{2}\right)E_{x0}^2 \tag{6}$$

$$\mathbf{F}_{\text{temp}} = -\hat{z}\,4\alpha\,n_m E_{x0}^2\frac{\tilde{t}}{c\tau} - \hat{y}\,4\alpha\,n_m E_{x0}^2 K^2\xi^2\frac{\tilde{t}}{c\tau} \tag{7}$$

We note that the gradient force has only a lateral component, whereas the scattering and temporal forces have two orthogonal components perpendicular to the electric field E_{x0} direction; along the beam propagation direction and in the lateral y-axis. The magnitudes of the gradient, scattering, and temporal forces depend on the laser beam intensity and on the spatial position in the trapping area, and in particular, the temporal force is also inversely proportional to pulse duration. The effect of the axial component field produced by the high-numerical aperture objective lens arises clearly in the gradient, scattering, and temporal forces in the term K^2. It is therefore interesting to calculate the forces in our real experimental case.

From knowledge of the size and refractive index of an individual polystyrene nanoparticle we calculated α to be $3.85\times10^{-34}\,\text{N m}^3\,\text{V}^{-2}$, and based on the Mie scattering theory [29] we obtained σ_p to be $3.5\times10^{-19}\,\text{m}^2$. By adopting the values of $K \approx 1.6/\pi$ for an objective lens with NA ≈ 0.9 [26,43] and $E_0 = (4P/\pi\omega_0^2 n_m\varepsilon_0 c)^{1/2} = 24.4\,\text{V}/\mu\text{m}$, (where $P = 350$ mW is the average power of the femtosecond laser, corresponding to laser power intensity of $1.05\times10^{12}\,\text{W/m}^2$ at the focal center), in Fig. 4(a) and (b) we show the plots of the calculated time-averaged gradient and scattering forces exerting on a spherical polystyrene nanoparticle as a function of the position x/ω_0. The lateral gradient force with the maximum being 0.14 pN at $x = 0.56\omega_0$ (shown in Fig. 4(a)) acts as a restoring force, which directs the nanoparticle towards the beam center as commonly observed in conventional optical trapping experiments [8,32]. The maximum value of axial scattering force is 1.6 fN at $x = 0$, and that of lateral scattering force is 0.08 fN at $x = 0.71\omega_0$, as shown in Fig. 4(b). Such the gradient and scattering forces of the time-averaged power of the mode-locked laser beam should also be applied for the cw laser beam. The calculated axial and lateral temporal forces, which apply only for the laser pulses, as a function of the time t/τ is plotted in Fig. 4(c). The plot reveals that the temporal forces fluctuate within the pulse envelope ($\tau = 90$ fs), similarly to the theoretical approach reported by Gordon [36] and Wang and Chai [40]. At the first half of the pulse, the axial and lateral component of the temporal force pushes the nanoparticles along the beam propagation and along y-axis, respectively, parallel to those of the scattering force. At the second half of the pulse the temporal force pushes the nanoparticles along the opposite directions. Interestingly, the maximum axial and lateral temporal forces were estimated to 12.3 fN and 1.7 fN, respectively, which are about 8 and 20 times larger than the respective component of scattering

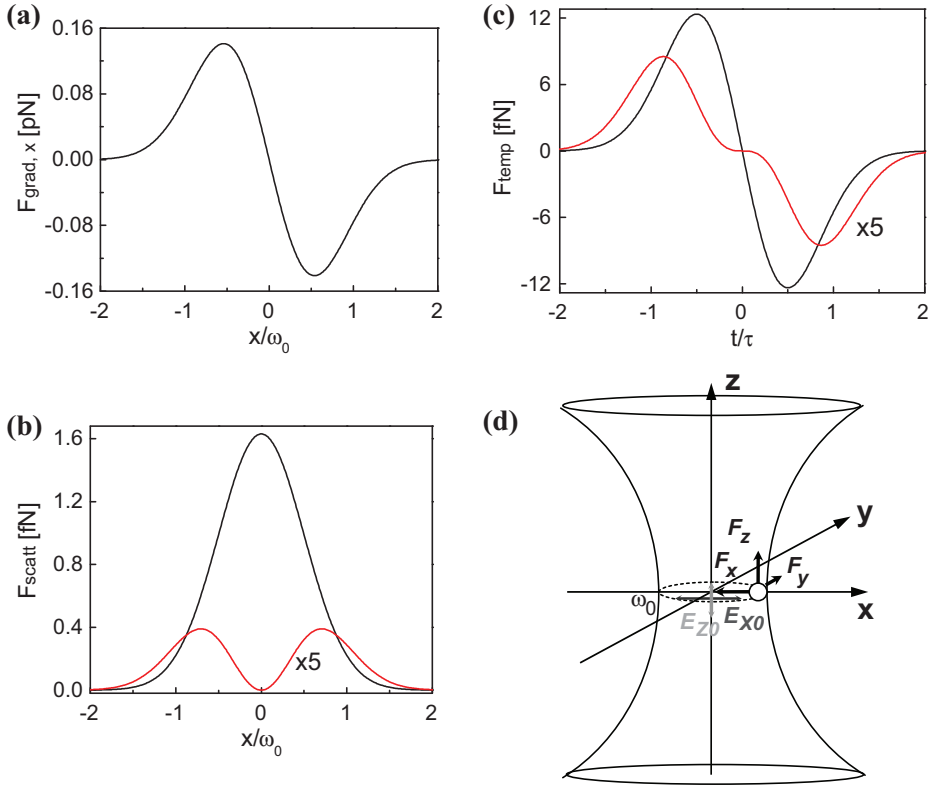

Fig. 4. Plots of calculated time-averaged gradient, scattering, and temporal forces acting on a polystyrene nanoparticle locating in the focal plane ($z = 0$) as a function of either the normalized lateral position of x/ω_0 or normalized time t/τ. (a) Lateral component of the gradient force, $\mathbf{F}_{grad}$, parallel to E_{x0}. (b) Axial (black) and lateral (red) components of the scattering force, F_{scatt}. (c) Axial (black) and lateral (red) components of the temporal force, F_{temp}. *Note*: for the sake of clarity, the lateral components of the scattering and temporal forces have been multiplied by a factor of 5. (d) A schematic illustration of the gradient, scattering, and temporal forces. *Note*: $\mathbf{F}_x = \mathbf{F}_{grad}$, $\mathbf{F}_y = F_{temp}\hat{y} + F_{scatt}\hat{y}$, $\mathbf{F}_z = F_{temp}\hat{z} + F_{scatt}\hat{z}$. (For interpretation of the references to color in this figure legend, the reader is referred to the web version of the article.)

force. Those gradient, scattering, and temporal forces are illustrated with a diagrammatic sketch in Fig. 4(d).

Considering that the optical trapping relies on the lateral gradient force, and that the magnitude of the lateral gradient force at the focal plane overcomes those of the scattering and temporal forces, the optical trapping of 50-nm diameter polystyrene spheres by the ultrashort laser pulses is realized. Such optical trapping of the nanoparticles is also supported by the estimated potential energy to be 13.8 k_BT (at 300 K) at the beam center, which is above the minimum criterion of a necessary potential energy to overcome thermal energetic for a stable optical trapping (10 k_BT) [8,28]. When the polymer nanoparticles escape from the optical trapping potential, they are readily scattered out of the focal spot by the resultant of axial and lateral components of both scattering and temporal forces. In particular, the lateral scattering and temporal forces, which are much larger in the front of the gravity of the nanoparticle (6.9×10^{-4} fN), should control the nanoparticle flows in the directions perpendicular to the light field polarization.

4.3. Comparison between radiation forces on the nanoparticles in femtosecond laser pulses and in CW laser

If the necessary potential energy of pulsed laser beams to trap the nanoparticles is related to their average power, similarly to the case of cw laser beams, we estimated that, under our experimental condition, the axial optical trapping can be achieved at minimum laser power of 250 mW. This is in agreement with our observation (264 mW). However, the optical trapping behavior of the nanoparticles by laser pulses dramatically differs from that by cw laser beam in terms of the number of trapped nanoparticles and the existence of scattered nanoparticles towards the directions controlled by the laser polarization. The higher number of nanoparticles trapped at the focal spot (Fig. 3(a)) by the laser pulses in comparison with that by cw mode indicates the higher optical trapping efficiency of the laser pulses, although the fluctuation of scattering light intensity at the focal spot takes place due to the dynamic particle motions during the pulse irradiation and pulse interval period. To clarify this issue, we consider the number of photons of the 800-nm laser beam transferred into the sample. For the laser pulses with an average power of 350 mW, the peak power of a single pulse is 4.9 nJ and the number of photons per second is 1.11×10^{23}, almost five orders higher than that of cw mode (1.41×10^{18}) for the same laser power, highlighting the impulsive peak power of the laser pulses in the front of cw mode. However, we should note that such a peak power in our experiment is much smaller than that to induce optical breakdown in water, which requires 0.1 μJ per pulse for 100 fs laser pulses [44], generating shockwave emission and cavitation bubble [44–47]. Unlike the polystyrene particles containing fluorescent dyes [38], the bare polymer nanoparticles in our experiments does not absorb efficiently two-photon excitation of the laser pulses, thus, they are not ablated by the laser pulses. We should also note that the polystyrene nanoparticle size is too much smaller than the beam waist to induce secondary convergence of the femtosecond laser pulses that can reduce the optical breakdown threshold as observed for polystyrene beads with a few tens of micron in diameter [27]. Thus, under our experimental condition we can rule out the possible contributions of shockwave, cavitation bubble (related to optical breakdown), or ablation, in the mechanism of the nanoparticle flows controlled by the laser polarization. Instead, as we proposed in Section 4.2, the lateral components of both scattering and temporal forces during the short pulse irradiation play an important role in the polarization-controlled nanoparticle flows.

The temporal force, which is not available in cw mode, pushes the nanoparticles in the fluctuating manner out of the focal center, inducing the dynamics of nanoparticle motion during the pulse duration. The particle motions may also induce convection of the liquid medium. Thus, combination of attractive and repulsive forces by the impulsive peak power, resulting in dynamic motions and diffusions of nanoparticles around the focal spot, makes optical trapping of laser pulses is more efficient than that of cw mode. In other words, under cw mode, the laser beam without modulation results in flat power, less controllable flows, less dynamic motions and diffusions of nanoparticles around the focal spot, and hence, less efficiency in optical trapping.

In order to evaluate whether a trapped nanoparticle can escape from the trap site by thermal motion during the pulse interval period between two pulses, we have considered the diffusion of a polystyrene nanoparticle in water. With 12.5 ns interval between two laser pulses (related to 80 MHz repetition rate) and diffusion coefficient in the order of $\sim 10^{-10}$ m^2 s^{-1} for 57-nm diameter polystyrene particle [48], we estimated the diffusion of the nanoparticles within the pulse interval period to be ~ 4 nm^2, which is much smaller than the focal spot size. We therefore could exclude the severe destabilization of the optical trapping due to the nanoparticle diffusion. Nevertheless, the diffusion during the interval between pulses may be attributed to the fluctuation of accumulated nanoparticles at the focal spot as indicated by the light intensity fluctuation in Fig. 3(a). Since the existence of nanoparticle aggregate at the focal spot can distort the light electric field, we proposed that a certain macroscopic shape of the accumulated nanoparticles allows the nanoparticle flows in one direction and the other shape in another direction. In this current experimental case, such a transition from one to another macroscopic shape of the accumulated nanoparticles takes place on the time-scale of seconds, not on the time-scale of the pulse duration. This also indicates that the change or destabilization of macroscopic shape of the accumulated nanoparticles is much slower than the fluctuation in the number of the optically trapped nanoparticles. The discrete probability distribution of the nanoparticle flows in one of the two opposite directions can be considered as a Poisson distribution.

Further, we interpret that pulse duration and repetition rate of laser pulses will be important parameters governing and bringing about the efficient optical trapping and polarization-controlled scattering of the dielectric spherical nanoparticles. This interpretation is in contrast to the optical trapping of 0.78 or 1.28 μm silica spheres, in which the optical trapping of the submicro- or microparticles by femtosecond laser pulses were reported to be just as effective as those by cw laser mode, and the optical trapping is independent on pulse duration within 12–40 fs over the repetition rate of 80 MHz [23,38]. This can be understood as we have interpreted our results based on instantaneous force on the 50-nm sized Rayleigh particles instead of total impulse transfer by the laser over the repetition cycle on such micron-sized particles, which are much larger than the beam waist implemented in those reports [23,38]. Finally, experiments with varying repetition rate and pulse duration of laser pulses, in addition to anisotropy, the concentration of the colloid, and the intrinsic polarizabilities of the Rayleigh colloidal particles as extensions of our current study are in progress in our laboratory, pursuing generality of the trapping and polarization-controlled scattering of dielectric nanoparticles by the tightly focused laser pulses, and the results will be reported elsewhere in near future.

5. Conclusion

We have presented optical trapping behavior of 50-nm sized dielectric spherical nanoparticles by the tightly focused ultrashort laser pulses. In addition to the single optical trap at the focal spot, the nanoparticles were also scattered from the focus spot to the surrounding area forming a partially opened folding fan-shaped bright locus in two opposite directions, in an alternating manner, perpendicular to the laser polarization. We have shown that as compared with the cw mode, the laser pulses can confine a larger number of the Rayleigh dielectric particles around the focal spot, highlighting the impulsive peak power of the ultrashort laser pulses. The temporal forces of the laser pulses, in addition to the scattering forces, readily push the nanoparticles out of the focal spot. In particular, the lateral scattering and temporal forces, which arise from the axial component of the electric field produced by the high numerical aperture of objective lens, can control the nanoparticle flows from the focal spot to the surrounding area. The controllable directions of the scattered nanoparticles by the polarization of laser pulses will open a new vista for controlling dynamical motion of nanoparticle assembly as well as for separation and sorting of nanoparticles with either different polarizabilities or scattering cross sections.

Acknowledgements

The financial supports from the Ministry of Education of Taiwan (MOE-ATU Project; National Chiao Tung University), the National Science Council of Taiwan (Grant No. NSC 100-2113-M-009-001), and Foundation of the Advancement for Outstanding Scholarship of Taiwan to H.M. are gratefully acknowledged.

Appendix A. Supplementary data

Supplementary data associated with this article can be found, in the online version, at doi:10.1016/j.jphotochem.2011.11.015.

References

[1] M.M. Martin, P. Plaza, N.D. Hung, Y.H. Meyer, Ultrashort pulse generation from the sweeping oscillator dye laser, in: E. Klose, B. Wilhelmi (Eds.), Ultrafast Processes in Spectroscopy, Springer-Verlag, Berlin, 1990.
[2] M.M. Martin, P. Plaza, Y.H. Meyer, J. Phys. Chem. 95 (1991) 9310.
[3] P. Plaza, M.M. Martin, Y.H. Meyer, M. Vogel, W. Rettig, Chem. Phys. 168 (1992) 365.
[4] M.M. Martin, P. Plaza, Y.H. Meyer, Chem. Phys. 192 (1995) 367.
[5] P. Changenet, H. Zang, M.J. van der Meer, M. Glasbeek, P. Plaza, M.M. Martin, J. Phys. Chem. A 102 (1998) 6716.
[6] P. Changenet-Barret, C. Loukou, C. Ley, F. Lacombat, P. Plaza, J.-M. Mallet, M.M. Martin, Phys. Chem. Chem. Phys. 12 (2010) 13715.
[7] J. Brazard, A. Usman, F. Lacombat, C. Ley, M.M. Martin, P. Plaza, L. Mony, M. Heijde, G. Zabulon, C. Bowler, J. Am. Chem. Soc. 132 (2010) 4935.
[8] A. Ashkin, J.M. Dziedzic, J. Bjorkholm, S. Chu, Opt. Lett. 11 (1986) 288.
[9] A. Ashkin, Proc. Natl. Acad. Sci. U. S. A. 94 (1997) 4853.
[10] P. Bartlett, S. Henderson, J. Phys.: Condens. Matter 14 (2002) 7757.
[11] S. Joudkazis, N. Mukai, R. Wakaki, A. Yamaguchi, S. Matsuo, H. Misawa, Nature 408 (2000) 178.
[12] H. Yoshikawa, T. Matsui, H. Masuhara, Phys. Rev. E 70 (2004) 061406.
[13] P. Borowicz, J. Hotta, K. Sasaki, H. Masuhara, J. Phys. Chem. B 101 (1997) 5900.
[14] J. Hofkens, J. Hotta, K. Sasaki, H. Masuhara, T. Taniguchi, T. Miyashita, J. Am. Chem. Soc. 119 (1997) 2741.
[15] T. Sugiyama, T. Adachi, H. Masuhara, Chem. Lett. 36 (2007) 1480.
[16] Y. Tsuboi, T. Shoji, N. Kitamura, J. Phys. Chem. C 114 (2010) 5589.
[17] K. Yuyama, T. Sugiyama, H. Masuhara, J. Phys. Chem. Lett. 1 (2010) 1321.
[18] T. Rungsimanon, K. Yuyama, T. Sugiyama, H. Masuhara, Cryst. Growth Des. 10 (2010) 4686.
[19] T. Rungsimanon, K. Yuyama, T. Sugiyama, H. Masuhara, N. Tohnai, M. Miyata, J. Phys. Chem. Lett. 1 (2010) 599.
[20] I.I. Smalyukh, J. Butler, J.D. Shrout, M.R. Parsek, G.C.L. Wong, Phys. Rev. E 78 (2008) 030701.
[21] K.C. Neuman, S.M. Block, Rev. Sci. Instrum. 75 (2004) 2787.
[22] M.A. van Dijk, L.C. Kapitein, J. van Memeren, C.F. Schmidt, E.J.G. Peterman, J. Phys. Chem. B 108 (2004) 6479.
[23] B. Agate, C.T.A. Brown, W. Sibbett, K. Dholakia, Opt. Express 12 (2004) 3011.
[24] L. Pan, A. Ishikawa, N. Tamai, Phys. Rev. B 75 (2007) 161305.
[25] M. Sanz, R. de Nalda, J.F. Marco, J.G. Izquierdo, L. Banares, M. Castillejo, J. Phys. Chem. C 114 (2010) 4864.
[26] Y. Jiang, T. Narushima, H. Okamoto, Nat. Phys. 6 (2010) 1005.
[27] Y. Jiang, C. Ma, I. Oh, Y. Hosokawa, H. Masuhara, Mod. Phys. Lett. B 24 (2010) 1739.
[28] Y. Harada, T. Asakura, Opt. Commun. 124 (1996) 529.

[29] C.F. Bohren, D.R. Huffman, Absorption and Scattering of Light by Small Particles, Wiley, New York, 1983.
[30] R.E.H. Miles, S. Rudic, A.J. Orr-Ewing, J.P. Reid, J. Phys. Chem. A 114 (2010) 7077.
[31] T. Uwada, T. Sugiyama, H. Masuhara, J. Photochem. Photobiol. A: Chem. 221 (2011) 187.
[32] P. Zemánek, A. Jonáš, L. Šrámek, M. Liška, Opt. Lett. 24 (1999) 1448.
[33] F. Qin, Y. Liu, Z.-Y. Li, J. Opt. 12 (2010) 035209.
[34] M.J. Bloemer, J.W. Haus, P.R. Ashley, J. Opt. Soc. Am. B 7 (1990) 790.
[35] K. Sasaki, M. Tsukima, H. Masuhara, Appl. Phys. Lett. 71 (1997) 37.
[36] J.P. Gordon, Phys. Rev. A 8 (1973) 14.
[37] L.-G. Wang, C.-L. Zhao, Opt. Express 15 (2007) 10615.
[38] J.C. Shane, M. Mazilu, W.M. Lee, K. Dholakia, Opt. Express 18 (2010) 7554.
[39] C. Hosokawa, H. Yoshikawa, H. Masuhara, Phys. Rev. E 72 (2005) 021408.
[40] L.-G. Wang, H.-S. Chai, Opt. Express 19 (2011) 14389.
[41] L.W. Davis, Phys. Rev. A 19 (1979) 1177.
[42] M. Koshioka, K. Sasaki, H. Masuhara, Appl. Spectrosc. 49 (1995) 224.
[43] L. Novotny, B. Hecht, Principles of Nano-optics, Cambridge Univ. Press, United Kingdom, 2006.
[44] A. Vogel, J. Noack, G. Hüttman, G. Paltauf, Appl. Phys. B 81 (2005) 1015.
[45] A. Vogel, V. Venugopalan, Chem. Rev. 103 (2003) 577.
[46] Y. Hosokawa, H. Takabayashi, S. Miura, C. Shukunami, Y. Hiraki, H. Masuhara, Appl. Phys. A 79 (2004) 795.
[47] Y. Hosokawa, M. Hagiyama, T. Iino, Y. Murakami, A. Ito, Proc. Natl. Acad. Sci. U. S. A. 108 (2011) 1777.
[48] P.-O. Gendron, F. Avaltroni, K.J. Wilkinson, J. Fluoresc. 18 (2008) 1093.